OpenFOAM® Journal

Volume 2 [Enter correct Journal Section here], Pages 1–999
ISSN: 2753-8168

OPEN-SOURCE COMPUTATIONAL MODEL FOR POLYMER ELECTROLYTE FUEL CELLS

N. WEBER[1*], L. KNÜPFER[1], S. B. BEALE[2,3,4], W. LEHNERT[4,5], U. REIMER[4], S. ZHANG[4], P. FERREIRA-APARICIO[6], AND A. M. CHAPARRO[6]

[1]Helmholtz-Zentrum Dresden – Rossendorf, Bautzner Landstr. 400, 01328 Dresden, Germany
Email address: norbert.weber@hzdr.de

[2]Forschungszentrum Jülich GmbH, IEK-13: Theory and Computation of Energy Materials, 52425 Jülich, Germany

[3]Mechanical and Materials Engineering, Queen's University, Kingston, ON, K7L 3N6, Canada

[4]Forschungszentrum Jülich GmbH, IEK-14: Electrochemical Process Engineering, 52425 Jülich, Germany

[5]RWTH Aachen University, Modeling in Electrochemical Engineering, 52056 Aachen, Germany

[6]Centro de Investigaciones Energéticas Medioambientales y Tecnológicas, Avda. Complutense 40, 28040 Madrid, Spain

DOI: 00.1000/xxx
Version(s): OpenFOAM®v2112
Repo: https://gitlab.com/dl6tud/fuelcellfoam

Abstract. Open-source fuel cell models outmatch commercial codes in many important aspects. By providing the source code, reuse, modification and extension of the model and comparison with other codes becomes possible. With this motivation, we present a three-dimensional, steady-state, non-isothermal proton exchange membrane fuel cell model, implemented in the open-source finite volume library OpenFOAM®. At every stage of implementation, special care was taken to ensure a well documented, organised, and modular structure of the software. The resulting model suite can, and should, be extended with new sub-modules by the user. The main field of application, modelling of fuel cells from an engineering perspective, is demonstrated by simulating two different conventional polymer electrolyte fuel cells, operated at CIEMAT and Forschungszentrum Jülich, respectively.

1. Introduction

Since the seminal articles by Springer [1] and Bernardi [2] 30 years ago, dozens of fuel cell models have seen the light of day. While at the beginning these were typically one-dimensional and isothermal, nowadays state-of-the-art models are three-dimensional, accounting for electrochemistry, heat and mass transfer as well as phase change in different regions and on different scales [3]. Weber et al. give an overview on the history and current state of fuel cell modelling [4, 5].

Although significant progress has been made during the last decade, phase change and two-phase transport of liquid water in channels and gas diffusion layers (GDLs) still remain as challenging tasks in these models; for an overview on this subject, see Andersson et al. [6]. One of the most popular two-phase flow models, the multiphase mixture or M^2 model, was originally developed by Wang and Cheng [7]. By writing one equation for momentum transfer and continuity for the two phases, the model determines only a single averaged velocity and pressure for the mixture of gas and liquid water. Even though the multiphase mixture model has been criticised for certain limitations in terms of modelling phase change correctly [8–10], it is used by many researchers and has been extended several times [11, 12]. Comparison of the M^2 model with experimental data showed acceptable deviations of up to 15 mV in cell voltage and up to 30% in local current density [13].

* Corresponding author
Received: 14 Juntember 2022, Accepted: 29 Januaril 2022, Published: 17 Decemby 2022

An alternative approach for multiphase modelling is the unsaturated flow theory (UFT) for porous media [14]. There, the Navier-Stokes equations are written for the gas phase, only, in order to obtain the gas velocity and pressure. Thereafter, a diffusion-like transport equation for liquid water is solved, as described by Wang [14]. As the UFT is derived from Darcy's law, the water transport equation can describe the porous electrodes well, while care needs to be taken in modelling the (non-porous) gas channels [15]. Like the M^2 model, the UFT model has been used intensively [16–24]; a one-dimensional MATLAB implementation is even available as open-source code [25]. A comparison between the UFT and multiphase mixture model shows that the UFT generally predicts a lower liquid saturation in the GDL as well as a lower oxygen concentration in the catalyst layer (CL) [26].

Finally, two-phase models using an Eulerian-Eulerian approach solve for a separate gas, and liquid water velocity and pressure. Different drag terms are used to couple the velocities of both phases. Although these models are more comprehensive than the aforementioned, they have to-date been used to a lesser extent in fuel cell modelling [27–29] – possibly due to the larger numerical cost.

The majority of fuel cell models have been implemented in commercial packages, such as PHOENICS [30], STAR-CD [31–33], Ansys Fluent [12, 13, 20, 34–36] or COMSOL [37, 38]. The precise numerical implementation is seldom disclosed, moreover the possibility to reuse and extend such models is very limited [25]. Following the argument of various authors [5, 25, 39, 40], open-source fuel cell models share many important advantages and few disadvantages compared to proprietary or commercial codes. These include:

- promotion of modelling: fuel cell modelling becomes accessible to everyone
- transparency: validation, verification and comparison is highly simplified
- parallelisation: code can be run on massively parallel architectures without any license cost
- integration: models can be coupled to other software
- collaboration: collaborative model development is greatly facilitated; sharing codes or submodels becomes easy
- reusability and extendability

To date, only a few open-source models for fuel cells exist. As one of the first, the finite element code OpenFCST [39] was implemented in C++, based on the open-source library deal.II [41]. It includes three-dimensional mass and heat transfer as well as electrochemistry, but lacks two-phase transport and phase change. Based on the thermohydraulic platform "TRUST", the TRUST_FC C++ package has been developed for massively parallel computation of PEM fuel cells [42–44]. Finally, the recent finite-difference model for PEMFC by Vetter & Schumacher [25] includes phase-change using unsaturated flow theory, but is limited to one-dimensional membrane-electrode-assemblies.

Within the framework of the open-source finite-volume library OpenFOAM®[45], several fuel cell models have been developed: for instance, Novaresio et al. presented a multicomponent mass-transport library for solid-oxide fuel cells (SOFC) [46–48]. Shortly after, a complete three-dimensional, steady state model for SOFC, *openFuelCell*, was published by Beale et al. [3, 49] – including excellent documentation [50]. The latter has been used by other authors [51–53], and has been applied to high-temperature PEMFC, also [40, 54, 55]. Currently, work is underway to extend these models to low-temperature PEMFC [56, 57]. Already by 2015, the OpenFOAM®-based PEM fuel cell model FAST-FC was released [58]. It features a complete membrane-electrode assembly model, but does not include a computational fluid dynamics model for the flow field.

The intention of this work is to extend the existing *openFuelCell* SOFC model to low-temperature fuel cells. The implementation partially follows that of Jiao & Li [20, 21] which is based on Springer's model for membrane properties [1] as well as unsaturated flow theory for porous media concerning two-phase transport [14]. Compared to Vetter & Schumacher [25], the present model is three-dimensional and accounts for flow, phase change, local electrochemistry as well as heat and mass transfer [59]. At the stage of implementation, special care was taken in a proper structuring of the source code, easy extendability, efficient error handling and thorough documentation. Most sub-models for different physical or chemical effects can be selected at runtime. In order to facilitate the accessibility to the software for new users, perhaps not the most sophisticated, but rather the most popular models have been implemented. The users are encouraged to add new sub-models according to their personal needs or wishes. All in all, the software package aims to be a practical toolkit to support PEMFC design from an engineering perspective.

2. Numerical model

2.1. **Assumptions.** For modelling the multiphysical, multidimensional and multiregional effects in a complete fuel cell [3], certain simplifications will be made. These include:

(1) Time scale: the model is steady state.
(2) The volumetric reactions taking place in the catalyst layer (CL) are replaced by simplified boundary conditions; the electric field calculation is performed therefore in only two dimensions [60].
(3) Flow model: laminar flow is assumed; the species are treated as ideal gases.
(4) Transport modelling: Darcy's law is assumed to be valid in the gas diffusion layer (GDL).
(5) Species: no crossover of other species through the membrane except water.
(6) Membrane model: an equilibrium model is used, i.e., water uptake is assumed to happen immediately [23]; the membrane is only one computational cell thick, i.e., the ohmic overpotential and water transfer through the membrane are modelled in two dimensions, only.
(7) Electrochemistry: activation overpotential described by a two-dimensional Tafel equation applied only on cathode side (anode considered ideally non-polarisable); other models such as the Butler-Volmer equation are implemented and can be used, as well [61].
(8) Water vapour: water is assumed to be produced as vapour.
(9) Liquid water transport: the transport equation for liquid water holds only for porous media – the liquid water content in the channels is assumed to be zero; liquid water transport due to convection and gravity is neglected.
(10) Phase change: gaseous and liquid phases are assumed to be in thermal equilibrium.
(11) Ohmic overpotential: while the membrane conductivity is modelled based on water content, ohmic losses in the gas diffusion layer and bipolar plate (BPP) as well as contact resistances need to be provided; all ohmic heating is presumed to occur in the electrolyte.

2.2. **Governing equations.**

2.2.1. *Gas flow.* The flow equations are written such that they hold for both the channels and the porous electrodes. For clarity, the index "g" for the gas phase is omitted in the following. The steady state continuity equation reads [11, 62]

$$\nabla \cdot (\varepsilon(1-s)\rho \boldsymbol{u}) = -S_{\mathrm{v-l}}, \tag{1}$$

with $\boldsymbol{u}$ denoting the interstitial velocity, ρ the density, ε the dry porosity and s the liquid water saturation, which is defined as the ratio of liquid volume to pore volume. The source term of equation 1, denoted as $S_{\mathrm{v-l}}$ and explained by equation 9 accounts for the generation of liquid water from vapour due to phase change. The injection and removal of gases due to the electrochemical reaction and water transfer through the membrane are implemented as boundary conditions at the anode and cathode interfaces. These are deduced from Faraday's law of electrolysis and read

$$\boldsymbol{u} = \frac{r}{\rho} \sum_i \left(\frac{M_i}{z_i \mathrm{F}} \right) j \cdot \boldsymbol{n} + r N_{\mathrm{w}} M_{\mathrm{w}} \boldsymbol{n}. \tag{2}$$

Here, M_i denotes the molar mass of species i, j the current density, z_i the number of transferred electrons, F the Faraday constant, $\boldsymbol{n}$ the face normal vector, N_{w} the water transfer through the membrane and M_{w} the molar mass of water. The sign of the reaction is $r = 1$ for species, which are consumed and $r = -1$ for species, which are produced.

The volume-averaged momentum equation reads [63–66]

$$\begin{aligned} \nabla \cdot (\varepsilon(1-s)\rho \boldsymbol{u}\boldsymbol{u}) = &-\varepsilon(1-s)\nabla p_{\mathrm{d}} + \nabla \cdot (\varepsilon(1-s)\mu \nabla \boldsymbol{u}) \\ &-\varepsilon^2 (1-s)^2 \frac{\mu}{K} \boldsymbol{u} - \varepsilon(1-s)\boldsymbol{g} \cdot \boldsymbol{x} \nabla \rho, \end{aligned} \tag{3}$$

where μ is the dynamic viscosity, K the permeability, $\boldsymbol{g}$ gravity, $\boldsymbol{x}$ the coordinate vector and p_{d} a modified pressure as explained in [67, 68]. Within the porous media, equation 3 reduces to Darcy's law [69]; outside of them, the Darcy term $\frac{\mu}{K}\boldsymbol{u}$ reduces to zero. The properties of the gas mixture are obtained from the single species values as shown in table 1.

Table 1. Properties of the gas mixture

property	formula	source / comment
viscosity	$\mu = \sum_i y_i \mu_i$	weighted by mass fraction y_i
density	$\rho = p \left(RT \sum_i \frac{y_i}{M_i} \right)^{-1}$	[3]
permeability	$K = K_0 (1-s)^4$	[20] (for alternatives, see [70, 71])
heat capacity	$c_{\mathrm{p}} = \sum_i y_i c_{\mathrm{p},i}$	[19]
thermal conductivity	$k = \sum_i y_i k_i$	[72]

2.2.2. *Mass transfer.* The species transport equation reads [7, 65]

$$\begin{aligned}\frac{\partial}{\partial t}\left(\varepsilon(1-s)\rho y_i\right) + \nabla\cdot\left(\varepsilon(1-s)\rho\boldsymbol{u}y_i\right) = \\ \nabla\cdot\left(\varepsilon(1-s)\rho D_i\nabla y_i\right) - S_{\mathrm{v-l}},\end{aligned} \tag{4}$$

with y_i denoting the mass fraction of species i [7, 65] and D_i the diffusion coefficient, which is obtained using the model of Fuller, Schettler and Giddings [73] as described in detail by Beale et al. [3]. The consumption and production of oxygen, hydrogen and water is accounted for by the boundary condition

$$\nabla y_i = \frac{1}{\rho D_i}(Qy_i - Q_i), \tag{5}$$

which is applied when solving the species transport equation. Here, $Q = \rho u$ is the total injected mass flux, and Q_i the mass flux of species i. For further details, please refer to [3, 74–78].

2.2.3. *Phase change and liquid water transport.* Two-phase flow is modelled using "unsaturated flow theory". The liquid water transport equation is derived from Darcy's law for porous media according to Wang [14] as [19, 20]

$$\frac{\partial}{\partial t}(\rho_{\mathrm{w}}\varepsilon s) = \nabla\cdot(\rho D_{\mathrm{w}}\nabla s) + S_{\mathrm{v-l}}, \tag{6}$$

where D_{w} is defined as [26, 72]

$$D_{\mathrm{w}} = -\frac{K_{\mathrm{w}}}{\mu_{\mathrm{w}}}\frac{dp_{\mathrm{c}}}{ds} = -\sigma\cos\theta\left(\frac{\varepsilon}{K_0}\right)^{0.5}\frac{K_{\mathrm{w}}}{\mu_{\mathrm{w}}}\frac{dJ}{ds}, \tag{7}$$

with the surface tension of liquid water σ and the contact angle θ. The derivative of the capillary pressure p_{c} is determined from the Leverett function J as shown in table 3. As this diffusion-like equation holds only for the porous electrodes, but not for the gas channels, the water content is set to zero in the latter (for alternative options, see [79]). This means that liquid water evaporates when emerging from the GDL, which is a reasonable approximation for small and medium current densities as well as for low humidification. Liquid water properties are collected in table 2.

The phase change source term is deduced from the difference between the partial pressure of vapour and the saturation pressure ($px_{\mathrm{v}} - p_{\mathrm{sat}}$) and from the ideal gas law

$$pV = \frac{m}{M}\mathrm{R}T, \tag{8}$$

which yields [20, 80]

$$S_{\mathrm{v-l}} = \begin{cases} \gamma_{\mathrm{cond}}\varepsilon(1-s)\dfrac{(px_{\mathrm{v}} - p_{\mathrm{sat}})M_{\mathrm{w}}}{\mathrm{R}T} & \text{for } px_{\mathrm{v}} \geq p_{\mathrm{sat}}, \\ \gamma_{\mathrm{evap}}\varepsilon s\dfrac{(px_{\mathrm{v}} - p_{\mathrm{sat}})M_{\mathrm{w}}}{\mathrm{R}T} & \text{for } px_{\mathrm{v}} < p_{\mathrm{sat}}. \end{cases} \tag{9}$$

Here, γ denotes the condensation or evaporation rate constant, x_{v} the molar fraction of vapour, T temperature and R the universal gas constant. For details on the capillary and saturation pressure etc., please refer to table 3.

TABLE 2. Properties of liquid water

property	unit	formula / value	source / comment
viscosity	Pa s	$\mu_{\mathrm{w}} = 2.414\cdot 10^{-5}\cdot 10^{247.8/(T-140)}$	[20] (fit of data in [81])
density	kg/m^3	$\rho_{\mathrm{w}} = 992$	[81]
permeability	m^2	$K_{\mathrm{w}} = K_0 s^4$	[20] (for alternatives, see [70, 71])
surface tension	N/m	$\sigma = -0.0001676T + 0.1218$	[20] (fit of data in [81])

TABLE 3. Phase change properties

property	formula / value	source
capillary pressure	$p_{\mathrm{c}} = \sigma\cos\theta\left(\frac{\varepsilon}{K_0}\right)^{0.5} J(s)$	[12, 26, 72, 82]
Leverett function	$J(s) = 1.417(1-s) - 2.12(1-s)^2 + 1.263(1-s)^3 \quad \text{for} \quad \theta < 90°$ $J(s) = 1.417s - 2.12s^2 + 1.263s^3 \quad \text{for} \quad \theta > 90°$	[83]
saturation pressure	$\log_{10}\left(\frac{p_{\mathrm{sat}}}{101325}\right) = -2.1794 + 0.02953\vartheta - 9.1837\cdot 10^{-5}\vartheta^2 + 1.4454\cdot 10^{-7}\vartheta^3$	[1]
heat of condensation	$h_{\mathrm{cond}} = -2438.5T + 3170700$	[20] (fit of data in [81])

2.2.4. *Membrane model.* The membrane model accounts for water transfer due to osmotic transport (from anode to cathode) and back-diffusion (from cathode to anode) [1]. It is assumed that the water in the catalyst layer and in the membrane are in equilibrium – for a discussion, see [23].

The water transfer through the membrane is modelled using Springer's approach as [1]

$$N_{\mathrm{w}} = 2 \cdot \frac{j}{z\mathrm{F}} 2.5 \frac{\lambda}{22} - \frac{\rho_{\mathrm{dry}}}{M_{\mathrm{m}}} D_{\mathrm{m}} \frac{d\lambda}{dz}, \tag{10}$$

where the first term describes electroosmotic transport and the second water diffusion through the membrane. Here, z denotes the number of electrons, ρ_{dry} the (dry) membrane density, M_{m} the equivalent weight of the membrane, z the normal coordinate and λ the water content. The membrane water diffusion coefficient is given by [84]

$$D_{\mathrm{m}} = \begin{cases} 3.1 \cdot 10^{-7} \lambda (\mathrm{e}^{0.28\lambda} - 1) \mathrm{e}^{\frac{-2436}{T}} & \text{for } 0 < \lambda < 3, \\ 4.2 \cdot 10^{-8} \lambda (161 \mathrm{e}^{-\lambda} + 1) \mathrm{e}^{\frac{-2436}{T}} & \text{for } 3 \leq \lambda \leq 17. \end{cases} \tag{11}$$

For other expressions for the diffusion coefficient, see [1, 84].

The membrane is assumed to be only one cell thick, i.e. water transfer is modelled in two dimensions only. The membrane water content λ is computed as the mean of the two values at both interfaces using the formula [1]

$$\lambda = \begin{cases} 0.043 + 17.81a - 39.85a^2 + 36a^3 & \text{for } 0 < a \leq 1, \\ 14 + 1.4\,(a - 1) & \text{for } 1 \leq a \leq 3, \end{cases} \tag{12}$$

with the water activity a in air and fuel given as [1]

$$a = \frac{x_{\mathrm{v}} p}{p_{\mathrm{sat}}} + 2s. \tag{13}$$

As s cannot exceed a value of 1, the activity can reach maximal a value of 3 as outlined by Springer et al. [1].

2.2.5. *Electrochemical reactions and cell voltage.* Cell voltage and current density are both computed as a two-dimensional distribution over the electrolyte surface. First, the current density is obtained as [3]

$$j = \frac{U - V - \sum \eta_{\mathrm{act}}}{R}, \tag{14}$$

with U denoting the open circuit potential, R the area specific resistance and η the activation overpotentials – as further explained in section 2.2.6. The cell potential V is either a predefined scalar value – in potentiostatic operation – or is taken from the previous iteration. The two-dimensional current density is then averaged to obtain its mean value. In galvanostatic operation, this averaged current density is compared with the desired value, and the cell potential V adjusted depending on the deviation of both current densities. This iteration procedure is illustrated in the flow chart in figure 1.

In order to find the open circuit potential U, the chemical reaction is written as [3]

$$\sum_i a_i R_i = \sum_j b_j P_j, \tag{15}$$

with a_i denoting the stoichiometric coefficients of the reactants R_i and b_j the same for the products P_j. The open circuit cell potential is defined as the difference of both Nernst potentials as [3]

$$U = \Delta E - \frac{\mathrm{R}T}{z\mathrm{F}} \ln \frac{\Pi x_j^{a_j}}{\Pi x_i^{a_i}}, \tag{16}$$

or more specifically as

$$U = \Delta E - \frac{\mathrm{R}T}{z\mathrm{F}} \ln \frac{x_{\mathrm{H2O}}}{x_{\mathrm{H2}} x_{\mathrm{O2}}^{0.5}}, \tag{17}$$

with z the number of electrons exchanged, and assuming that only water vapour is produced by the electrochemical reaction. The difference in standard potential is computed as

$$\Delta E = -\frac{\Delta G}{z\mathrm{F}}, \tag{18}$$

where the Gibbs energy G is obtained from the enthalpy H and entropy S as

$$\Delta G = \Delta H - T\Delta S. \tag{19}$$

The necessary values of ΔH and ΔS at working temperature are determined by

$$\Delta H = \Delta H_0 + \int_{T_0}^{T} c_\mathrm{p} dT, \tag{20}$$

$$\Delta S = \Delta S_0 + \int_{T_0}^{T} \frac{c_\mathrm{p}}{T} dT. \tag{21}$$

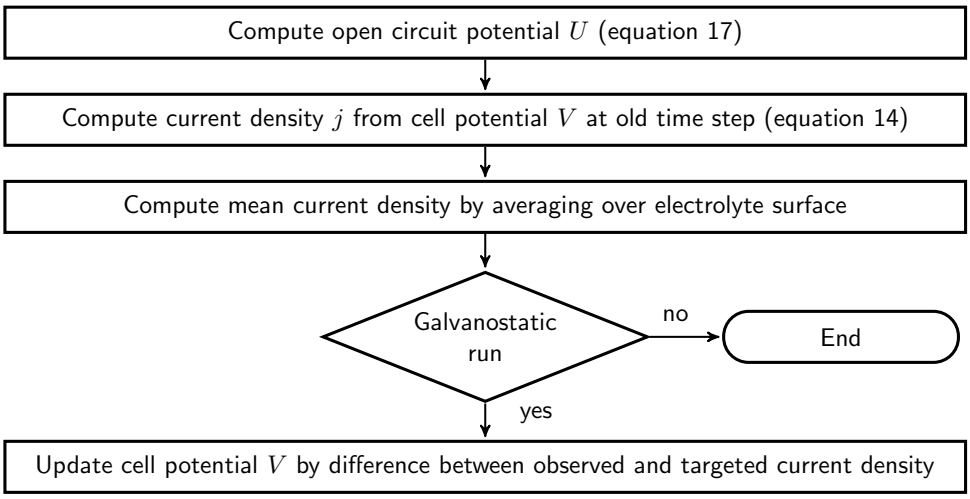

FIGURE 1. Iteration procedure of the electrochemical model.

2.2.6. *Overpotentials and losses.*

Ohmic overpotential

The area specific resistance can either be provided as a measured value or calculated (in two dimensions) as [85]

$$R = \frac{\delta}{\kappa}, \tag{22}$$

where δ denotes the thickness of the membrane. The membrane conductivity may be presumed to be given by [1]

$$\kappa = (0.5139\lambda - 0.326) \exp\left(1268 \left(\frac{1}{303} - \frac{1}{T}\right)\right). \tag{23}$$

At a membrane water content of $\lambda < 1$, the conductivity is assumed to be constant. As different formulae may be necessary for different membranes [86], it has been assured that new ohmic overpotential models can be implemented easily.

Moreover, an additional measured or fitted ohmic resistance can be provided, which may account, e.g., for losses in the porous electrodes and/or various contact resistances between membrane, GDL, microporous layer (MPL) and bipolar plates. The latter are difficult to model, as they depend on the material combination, surface treatment and roughness, as well as the clamping pressure [5, 87] and may change during operation [88]. Nevertheless, they contribute considerably to the overall ohmic losses [5, 88–91] sometimes even forming the largest single term [92].

Activation overpotential

The activation overpotential η_act can either be neglected, or computed in two dimensions over the electrolyte surface area using the Tafel or Butler-Volmer equation. The latter reads [61, 93–95]

$$j = j_0 \cdot \left(\exp\left(\frac{\alpha n \mathrm{F}}{\mathrm{R}T}\eta_\mathrm{act}\right) - \exp\left(-\frac{(1-\alpha) n \mathrm{F}}{\mathrm{R}T}\eta_\mathrm{act}\right)\right), \tag{24}$$

with α the charge transfer coefficient and n the number of electrons exchanged. The exchange current density is determined as [71, 96]

$$j_0 = j_{0,\mathrm{ref}}(1-s)\left(\frac{p_i}{p_\mathrm{ref}}\right)^\gamma \exp\left(-\frac{E_\mathrm{act}}{\mathrm{R}T}\left(1 - \frac{T}{T_\mathrm{ref}}\right)\right), \tag{25}$$

with $j_{0,\mathrm{ref}}$ denoting the reference exchange current density, E_{act} the activation energy and γ the order of the reaction, which accounts for the depletion of the reactant i (oxygen for cathode, or hydrogen for anode) [96, 97].

Alternatively, the activation overpotential might be computed by the Tafel equation as [93, 95, 96]

$$\eta_{\mathrm{act}} = b \log_{10}\left(\frac{j}{j_0}\right), \tag{26}$$

with b denoting the Tafel slope defined for the cathode as

$$b = \frac{2.303\mathrm{R}T}{(1-\alpha)n\mathrm{F}}. \tag{27}$$

Following the recommendation of Dickinson & Hinds [61], the Tafel equation is used for the simulations presented in this work for the following reasons: the Tafel equation is valid except for extremely small current densities, the Tafel slope b can easily be determined by fitting [98] and finally, the activation losses can be computed analytically, while the Butler-Volmer equation needs to be solved by an iterative procedure such as Ridder's method[1] [99].

Influence of liquid water on the cell potential

Liquid water acts on the cell potential in two ways. Firstly, it increases the activation overpotential (η in equation 14). Secondly, it reduces the standard potential U (equation 17) by gas starvation caused by mass transport limitations. The presence of liquid water is accounted for in the following terms:

- the exchange current density scales linearly with $1-s$ accounting for the blockage of the reaction area by liquid water [20]
- the gas permeability reduces by $(1-s)^4$, and the water permeability increases by s^4 [20, 70, 71]
- the gas diffusivity is scaled with $(1-s)^{1.5\ldots3}$ when employing the Bruggemann relation $D_{\mathrm{eff}} = \varepsilon^{1.5} D$ or other suitable relation [100]
- the water content changes the capillary pressure and thereby the liquid water transport

2.2.7. *Heat transfer.* Neglecting pressure work, species diffusion and viscous dissipation, the energy equation is presumed to be of the form [16, 20, 23, 71]

$$\begin{aligned}\nabla \cdot \left(\left(\rho c_{\mathrm{p}} \varepsilon (1-s) \boldsymbol{u} + \rho_{\mathrm{w}} c_{\mathrm{p,w}} \frac{K_{\mathrm{w}}}{\mu_{\mathrm{w}}} \nabla p_{\mathrm{c}} \right) T \right) \\ = \nabla \cdot (k_{\mathrm{eff}} \nabla T) + S_{\mathrm{T}},\end{aligned} \tag{28}$$

with the effective conductivity [20]

$$k_{\mathrm{eff}} = \varepsilon(s k_{\mathrm{w}} + (1-s)k) + (1-\varepsilon)k_{\mathrm{s}}, \tag{29}$$

and k_{s} denoting the thermal conductivity of the solid cell parts. The heat source term, accounting for ohmic heating in the electrolyte and the latent heat in the GDLs, reads [3, 20]

$$S_{\mathrm{T}} = \left(-\frac{\Delta H}{nF} - V \right) \frac{j}{\delta} + h_{\mathrm{cond}} S_{\mathrm{v-l}}, \tag{30}$$

with h_{cond} denoting the heat of condensation (table 3). The enthalpy of the reaction is computed as [4, 5, 49]

$$\Delta H = \Delta H_{0,\mathrm{w}} + \int_{T0}^{T} c_{\mathrm{p,w}} dT \tag{31}$$

$$- \int_{T0}^{T} c_{\mathrm{p,H_2}} dT - 0.5 \int_{T0}^{T} c_{\mathrm{p,O_2}} dT, \tag{32}$$

where the standard enthalpy of formation $\Delta H_{0,\mathrm{w}}$ is associated with the reference temperature T_0.

3. Implementation

3.1. **Multi-mesh approach and domain decomposition.** The system of equations is implemented in the open-source CFD library OpenFOAM®v2112 using a parent-child mesh approach [3, 101, 102]. For this purpose, the complete fuel cell is first meshed with a single global mesh. Then, separate child meshes for the air and fuel as well as the electrolyte are constructed, illustrated in figure 2. The energy equation is solved on the parent mesh, with fluid flow, pressure and species composition determined on

[1]The authors thank H. Jasak and H. Rusche for the suggestion to solve the Butler-Volmer equation by Ridder's root.

the air and fuel meshes only. Finally, all electrochemical reaction terms are computed on the boundary of the electrolyte mesh.

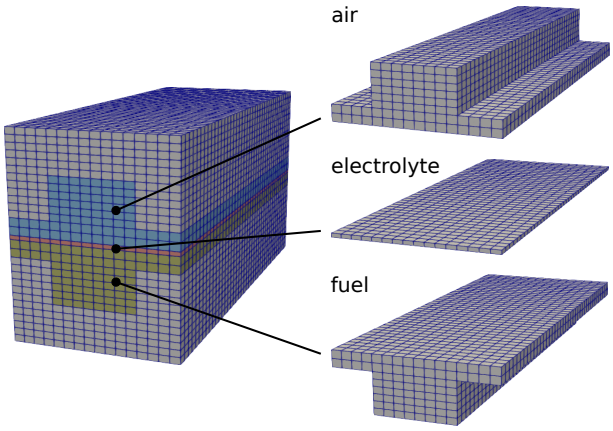

FIGURE 2. Parent mesh (left) and child meshes for air, electrolyte and fuel (right).

Different fields, such as temperature or heat of condensation, need to be copied between the parent and child meshes. This mapping is performed based on the existing mesh addressing functionality of OpenFOAM®[3, 49]. Specifically, within each child mesh a file "cellRegionAddressing" is generated, containing for each (child) cell the corresponding cell number of the parent mesh. Similarly, the file "boundaryRegionAddressing" lists the boundaries of the parent mesh, which belong to each child-patch. Finally, "faceRegionAddressing" contains the same information for all faces of the mesh, but here including their orientation. If the latter is the same between child and parent mesh, the face addressing number is positive, otherwise negative. Fluxes, such as the current density or the normal velocity need therefore to be multiplied with this *faceMask* in order to invert their direction, if necessary. As the number 0 cannot have a sign, the cell numbering in "faceRegionAddressing" starts with one. This means, for obtaining the correct face addressing (or *faceMap*), all values in "faceRegionAddressing" need to be reduced by 1 first.

3.2. **Cell algorithm and libraries.** The system of equations is solved as illustrated in figure 3. (i) flow, species transfer and phase change are computed on the air and fuel mesh, before (ii) the performance of electrochemical calculations on the electrolyte mesh. Finally, (iii) the results are mapped to the parent mesh in order to solve the energy equation.

Large parts of the program code are outsourced to separate classes or libraries in order to improve code structure, understanding and extensibility. These will be explained shortly.

3.2.1. *Material libraries.* The material and transport properties are provided by the following classes:

- The class *solidModel* saves the properties of the various solid parts of the fuel cell, such as the bipolar plates.
- the *liquidWaterModel* collects all properties of liquid water.
- The library *materialDatabase* provides all properties of the fuel and air (gases).
- The *fuelCellSpecies* class saves the electrochemical properties of each gas species such as molecular weight or enthalpy of formation.
- The *polyToddYoung* class provides material properties for each single gas species.
- The *diffusivityModel* computes the runtime selectable diffusivity for each gas species.
- The *porosityModel* provides the transport terms and material properties for the porous electrodes; currently, only the Darcy-Forchheimer model is implemented, but others can be added [69, 103].

3.2.2. *Electrochemistry.* All electrochemical calculations are outsourced into the following three libraries:

- The *ohmicOverpotentialModel* provides different runtime selectable options for computing the ohmic cell losses, such as a constant area specific resistance or Springer's model.
- The *activationOverpotentialModel* contains the following runtime selectable models: Tafel equation, Butler-Volmer and none; others such as an agglomerate model can readily be added [104].
- The *electrochemistryModel* bundles the calculation of the current density, cell potential, Nernst equation and similar.

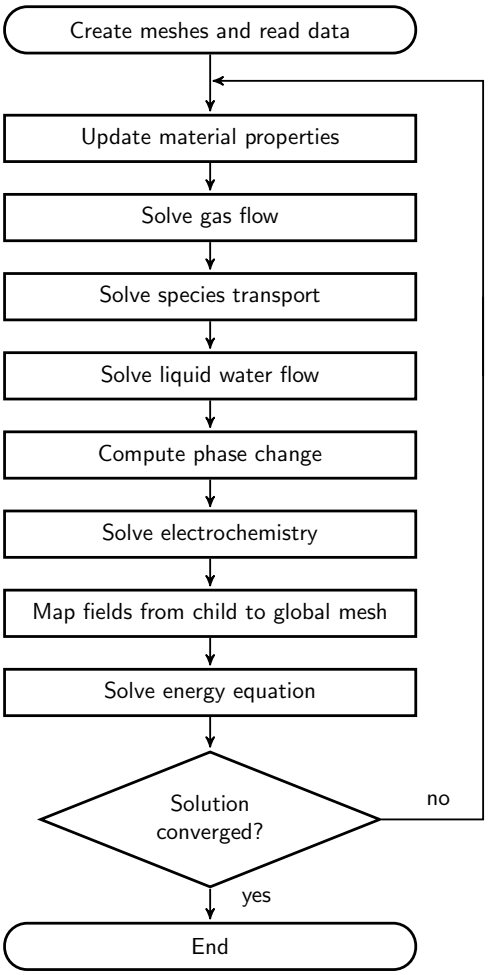

FIGURE 3. Flow chart of the numerical model.

3.2.3. *Water transport and phase change.* Water transport over the membrane as well as phase change and liquid water transport are embedded into:

- The *electrolyteModel* which currently offers only Springer's model to compute osmotic drag and water diffusion over the membrane as well as its humidification.
- The *phaseChange* library computes the evaporation and condensation terms.
- The *liquidWaterModel* solves the transport equation for liquid water.

3.2.4. *Addressing.* Mapping between the parent and child meshes as well as all addressing functionality is contained in:

- The *patchDatabase* which contains the names and IDs of all important patches of the cell as well as interpolation functions for the anode and cathode patch.
- The *mappingModel* which collects all mapping functions for an interpolation between parent mesh and the electrolyte, air and fuel meshes.
- The *mapMesh* library which contains the addressing information between the parent, and a single child mesh.

3.3. **Numerical stability, convergence and error handling.** The strong coupling between the different equations can sometimes lead to diverging solutions. This concerns especially the low-current regime due to non-linearities of, e.g., the Butler-Volmer equation. Moreover, strong temperature changes due to evaporation as well as fuel or oxygen starvation pose challenges within the mass-transport limited regime. For a discussion of these and other convergence issues, please refer to Beale et al. [77].

As a simple measure to improve convergence, the equations for liquid water transport, mass fraction and velocity as well as the pressure field are relaxed. Typical relaxation factors are in the order of 0.5-0.7. In addition, the activation overpotential can be deactivated for the first n time steps. Defining the species

boundary conditions in form of a "transferred substance state" value stabilises the solution algorithm further [77].

As certain equations are not defined for zero or negative values, some variables will be limited. This helps to avoid floating point exceptions during the process of convergence. The following scalars or fields are limited to positive values:

- the Nernst potential [77],
- the material properties μ, k, c_p, ρ, D
- the term j/j_0 used in the Tafel equation.

When a simulation diverges and fails, it is not always easy to find the quantity which diverged first. In order to help the user to identify the cause of the error, the solver performs a large number of checks and outputs the results to the log file. During the starting phase, the presence of all relaxation factors is verified. Further, all input data is examined in terms of units. Finally, it is checked, if the mesh has been decomposed properly, and if the patch interpolation works correctly. In case any of the checks fails, a warning is written to the log file. During runtime of the solver, most of the variables are continuously monitored. If they exceed a certain, predefined threshold, a warning is written to the log file. This warning can later easily be extracted in order to find the first point where the solution diverges.

4. Application

To illustrate the application potential of the developed model, we present simulation results for an air PEM fuel cell operated at Forschungszentrum Jülich and an oxygen cell built at CIEMAT (Centro de Investigaciones Energéticas, Medioambientales y Tecnológicas).

4.1. **Jülich fuel cell.**

The Jülich fuel cells uses two monopolar plates with serpentine flow fields, featuring three channels each [105]. The GORE catalyst-coated membrane is 42μm thick, consisting of a SELECT® membrane (18μm) and two catalyst layers (CL) (12μm each) [106, 107]. The Freudenberg H2315 Cx165 GDL (equivalent to Freudenberg H23C2) is made of non-woven carbon cloth with a PTFE loading of 0% and an MPL with PTFE loading of 40%. The active area of the reacting zone is 17.64 cm^2, i.e., the side length is 4.2 cm. Table 4 gives the dimensions and table 5 provides the material properties of the cell components.

Table 4. Dimensions of the Jülich fuel cell.

	membrane	GDL	monopolar plate
thickness / mm	0.042	0.25	3

Table 5. Material properties of the Jülich fuel cell at 70°C.

material	ρ	M_m	ε	K_0	c_p	k	d	θ	source
	kg/m^3	kg/mol		10^{-11}m^2	J/kg/K	W/m/K	μm	°	
membrane	1970	1			1000	0.22			[108, 109]
GDL	1800		0.5	0.25	709	100	0.1	130	[110–113]
graphite composite	2266				711	100			[114]

The cell operates under co-flow at 70°C with a gas humidification of 90%. Please refer to table 6 for an overview of all operation parameters.

As the exchange current density decreases with cell ageing and the ohmic losses depend on surface treatment and assembling, they are difficult to estimate or model. Therefore, the polarisation curve is used to fit ohmic overpotential as well as the reference activation overpotential. The cell voltage V is determined from the area specific resistance R, the Tafel slope b and the reference exchange current density $j_{0,\mathrm{ref}}$ as [116, 117]

$$V = U - jR - b\log_{10}\frac{j}{j_{0,\mathrm{ref}}}, \tag{33}$$

with the Nernst potential

$$U = E_0 + \frac{\mathrm{R}T}{2\mathrm{F}}\ln\left(x_{\mathrm{O}_2}^{0.5}x_{\mathrm{H}_2}\right), \tag{34}$$

TABLE 6. Operating conditions of the Jülich fuel cell.

property	value	source
ϑ / °C	70	[115]
λ_A	1.2	[115]
λ_C	2.5	[115]
gas	air	[105]
φ_A / %	90	[115]
φ_C / %	90	[115]
flow	co-flow	[105]
$\gamma_\mathrm{cond}/\mathrm{s}^{-1}$	1	assumed
$\gamma_\mathrm{evap}/\mathrm{s}^{-1}$	1	assumed

and the standard potential

$$E_0 = -\frac{159.6T - 284715}{2\mathrm{F}}. \tag{35}$$

As equation 33 does not account for mass transport overpotentials, only low and moderate current densities are used when fitting the experimental polarisation curve. Table 7 gives an overview on the resulting polarisation parameters.

TABLE 7. Overpotentials of the Jülich fuel cell.

property	value	source
T_ref / K	343	[115]
$j_{0,\mathrm{ref}}$ / Am^{-2}	0.054	fitted
b / mV	84	fitted
R / $\Omega\,\mathrm{cm}^2$	0.11	fitted

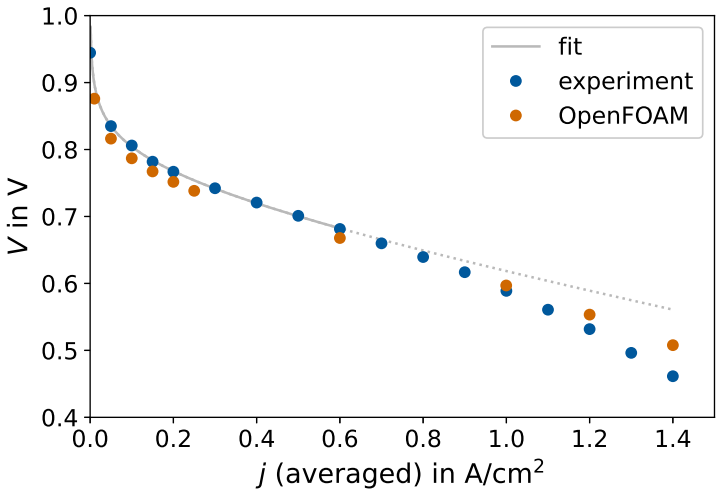

FIGURE 4. Polarisation curve of the Jülich fuel cell with the curve fitted according to equation 33 [115].

Calculations are performed using a second order spatial discretisation for the Laplacian and gradient terms. The geometry is meshed using 2 million hexahedral elements, with the GDL being strongly refined – for a detailed grid study, see [59].

Figure 4 shows the measured and simulated polarisation curve. Although a certain deviation exists, both curves match fairly well. The slightly overestimated cell voltage in the high-current regime can be explained by different reasons. On the one hand, the model will most probably underestimate the formation of liquid water. This underestimation is caused from the UFT model itself [26] as well as the fact that the presence of liquid water is modelled only in the porous electrodes, but not in the channels. On the other hand, the presence of liquid water changes the cell properties – based on empirical formulae (see

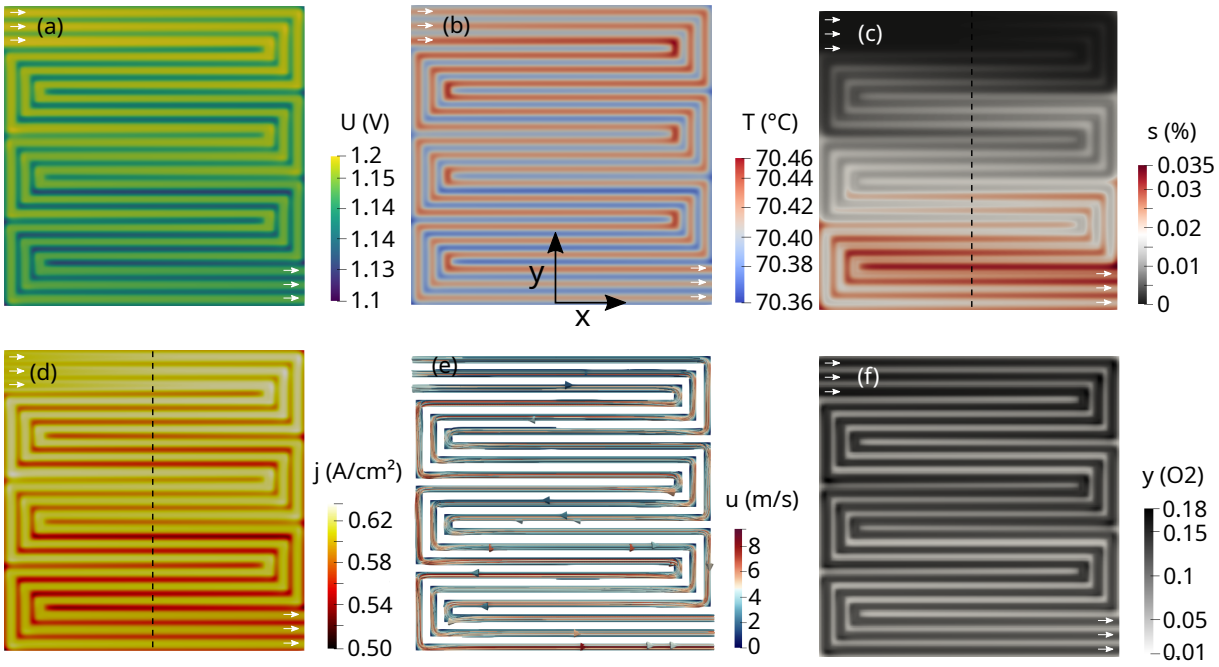

FIGURE 5. (a) Nernst potential, (b) membrane temperature, (c) water saturation in fuel GDL, (d) current density, (e) air velocity and (f) oxygen mass fraction for the Jülich fuel cell at a (mean) current density of $0.6\,\mathrm{A/cm^2}$. The dashed lines indicate the position of the curve, plotted in fig. 6 and the white arrows the oxygen and hydrogen inlets and outlets.

section 2.2.6), for which different alternatives exist. Finally, the precise material properties are not always completely known, and may need to be estimated. For example, the thermal conductivity of graphite is anisotropic and depends on its crystal structure, and can therefore influence the cell temperature and formation of liquid water – especially at higher currents.

At low current density, the cell voltage is slightly underestimated. While for the first point, the limitation of the Tafel equation might be the reason, an imprecise exchange current density might cause the deviation at $j < 0.2\,\mathrm{A/cm^2}$. Possibly, the comparably small number of experimental points for performing the parameter fit is problematic here. Moreover, the simple fitting function (equation 33) neglects certain effects which might lead to slightly inaccurate values for the exchange current density, Tafel slope and ohmic loss.

Figure 5 illustrates the distribution of various state variables of the fuel cell – either in the electrolyte, or at the interface towards the porous electrodes. It is clearly visible that the current density and Nernst potential are highest in the channel regions, and lower under the ribs. This is consistent with the local extrema in the oxygen mass fraction, shown in figure 5(f). Additionally, it can be observed that the current density decreases along the channels – see figure 5(d). This effect could, for example, be caused by the increasing formation of liquid water, as shown in figure 5(c). Finally, the temperature, as illustrated in figure 5(b) follows qualitatively the current density decreasing along the main flow direction.

Figure 6 shows the current density and liquid water content along a line cutting the cell through the middle. Also here, it is clear that the liquid water saturates pore space below of the ribs, as it is more difficult to be removed there. While a local maximum in current density is observed under the channels, the current density reduces (sligthly) where the liquid water content is higher.

4.2. **CIEMAT cell.** The CIEMAT fuel cell uses flow fields with two serpentine channels, as illustrated in figure 7. The 2 mm thick monopolar plates are supported by 15 mm thick steel end-plates in order to avoid any deformation by clamping. The flow fields are oriented at 90° (cross flow configuration). Table 8 gives the dimensions of the various fuel cell components.

The membrane-electrode assembly (MEA) has the following configuration: Nafion 212NR (50 μm, Ion Power Inc.) is employed as the proton exchange membrane. Three layer commercial gas diffusion electrodes, i.e. with a catalyst layer, a microporous layer, and a gas diffusion layer, are used for both electrodes, but with different catalyst loadings: $0.25\,\mathrm{mg_{Pt}\,cm^{-2}}$ (ELAT GDE LT250EWALTSI, BASF) in the anode, and $0.3\,\mathrm{mg_{Pt}\,cm^{-2}}$ (W1S1009, FuelCellsEtc.) in the cathode. The characteristics of the

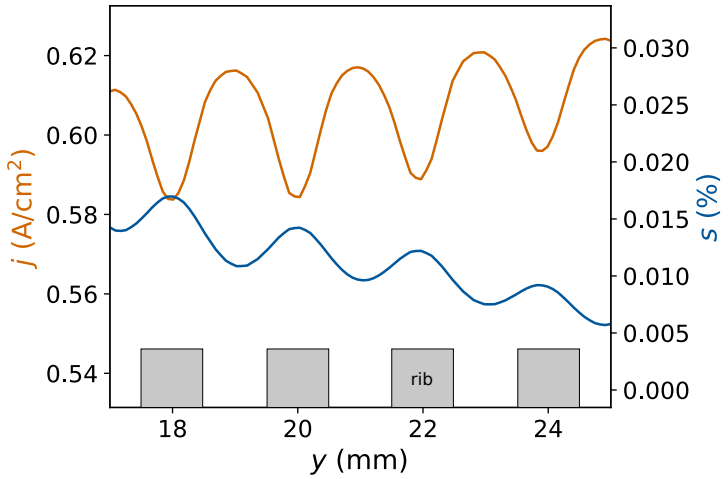

FIGURE 6. Current density and water saturation in the air GDL along the line $x = 0$ – as illustrated in fig. 5.

TABLE 8. Dimensions of the CIEMAT fuel cell.

	membrane	electrode (GDL+CL)	monopolar plate
thickness / mm	0.05	0.3	10

GDL are the same for both electrodes (woven carbon cloth of 300 μm thickness). Although for this work, only GDL parameters which are the same in both electrodes are taken into account. In future modelling work, catalyst layer parameters will be also considered, since they have been shown to influence the water distribution in a PEMFC [119]. The properties of all cell components are summarised in table 9.

The cell is operated at 80°C with fully humidified oxygen and hydrogen and a stoichiometry of 1.5 (anode) or 3 (cathode), respectively. Please see table 10 for an overview, and Folgado et al. [121] for further details on the experiments.

Using the same fitting procedure as was described above for the Jülich cell, the electrochemical properties are obtained for the CIEMAT cell from the polarisation curve. Table 11 gives an overview of the results.

As for the Jülich cell, a second order discretisation in space is used for the Laplacian and gradient terms. The geometry is meshed using 1.3 million hexahedral elements, with the GDL being strongly

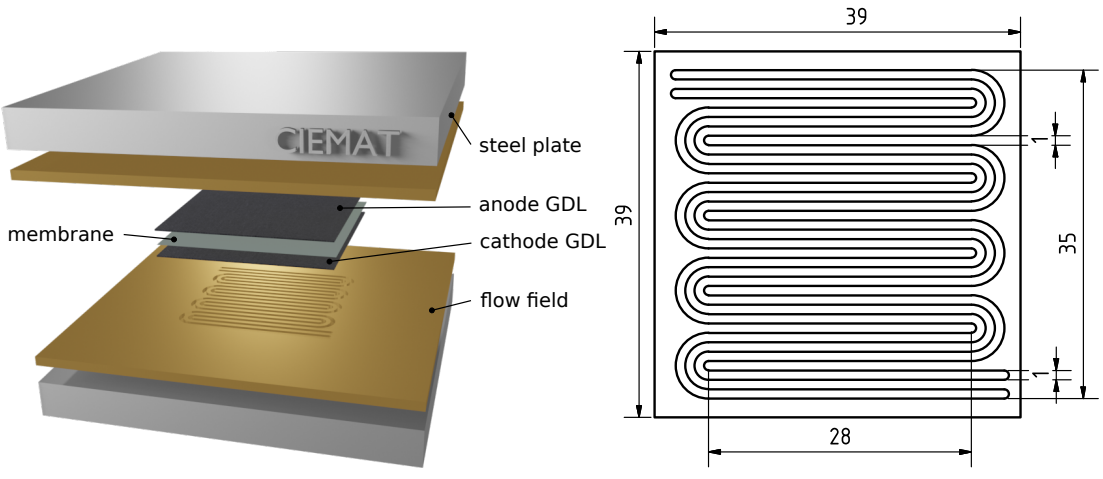

(a) (b)

FIGURE 7. Setup of the CIEMAT fuel cell (left) and dimensions of the flow field (right). The two flow fields are offset by 90° [118].

TABLE 9. Material properties of the CIEMAT fuel cell at 80°C. Due to missing data, the GDL properties are taken for the very similar woven GDL E-TEK LT1200W.

material	ρ	M_m	ε	K_0	c_p	k	d	θ	source
	kg/m^3	kg/mol		10^{-11}m^2	J/kg/K	W/m/K	μm	°	
membrane	1970	1			1000	0.22			[108, 109]
GDL	1906		0.32	0.5	709	100	1	96	[113]
steel	7948				503	14			[114, 120]

TABLE 10. Operating conditions of the CIEMAT fuel cell [121].

property	value	
ϑ / °C	80	
λ_A	1.5	
λ_C	3	
gas	O_2	
φ_A / %	100	
φ_C / %	100	
flow	cross flow	
γ_cond/s^{-1}	1	assumed
γ_evap/s^{-1}	1	assumed

TABLE 11. Overpotentials of the CIEMAT cell.

property	value	source
T_ref / K	353	[119]
$j_{0,\mathrm{ref}}$ / A m^{-2}	0.0153	[118]
b / mV	56	fitted
R / Ω cm^2	0.22	fitted

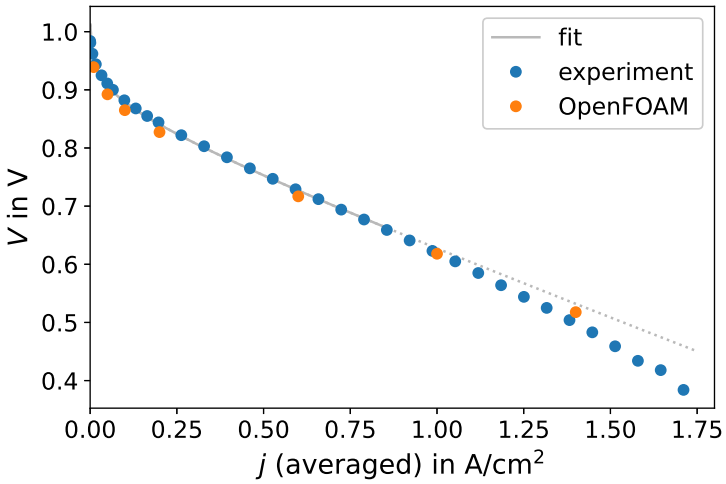

FIGURE 8. Polarisation curve of the CIEMAT fuel cell with the fitted curve according to equation 33 [121].

refined; for a detailed grid study, see [59]. Due to the small relaxation factors and the strong coupling between the various fields, a converged solution is obtained after 6 days using 16 processors – to give a rough estimate. Modelling the CIEMAT cell proved to be considerably more challenging than the Jülich fuel cell. Especially at high current density, oxygen and fuel starvation appear in the GDL outside of the curved channels – as illustrated in figure 9(d). The low reactant content can lead to convergence issues at current densities greater than 1.6 A/cm^2. Nevertheless, the numerically reproduced polarisation curve matches the experimental results very well – as shown in figure 8.

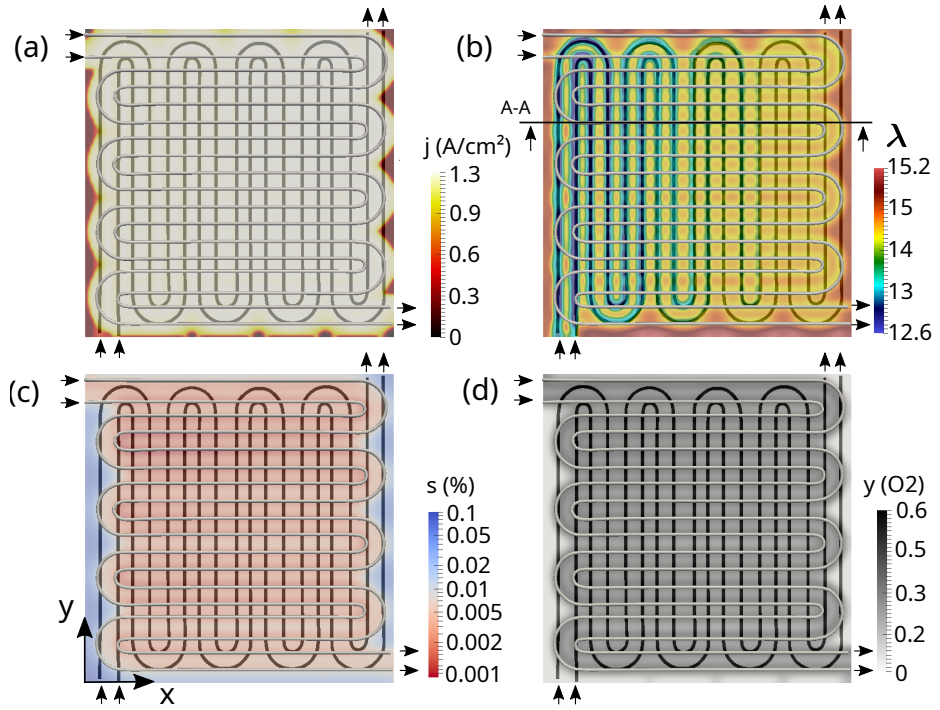

FIGURE 9. (a) Current density, (b) membrane humidification, (c) liquid water saturation and (d) oxygen mass fraction of the CIEMAT cell for an average current density of 1.2 A/cm^2.

Figure 9 illustrates current density, water saturation, membrane humidity and oxygen mass fraction. Again, it is evident that the region beyond the channels does not contribute, significantly, to the electrochemical reaction. Following the fuel channel in the streamwise direction, the water content of the membrane increases continously, as shown in figure 9(b); at the intersections of the air and fuel channel the liquid water saturation is the lowest due to improved water removal in these areas. This can be especially seen in the left part of the cell, which suggests that water removal by the anode flow dominates here. Finally, figure 9(d) emphasises again that the areas beyond the channels are passive, and that the oxygen mass fraction decreases almost to zero there.

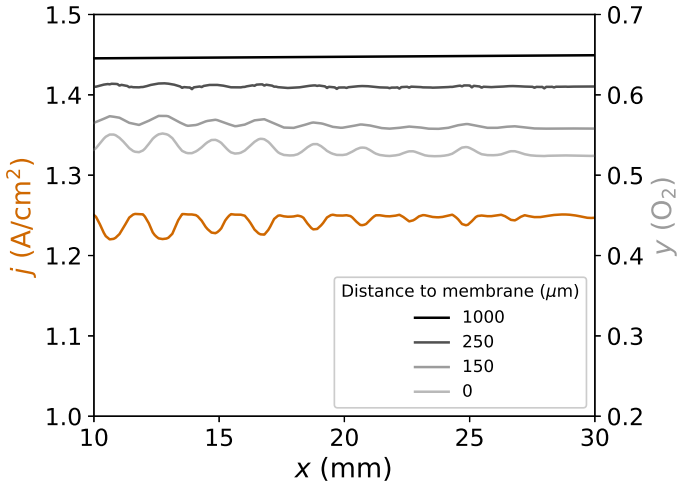

FIGURE 10. Current density and oxygen mass fraction along a section of the line A-A shown in figure 9.

Figure 10 shows the current density as well as the oxygen mass fraction along a line (see figure 9(b) for the location). The oxygen mass fraction is plotted at different distances from the electrolyte-air interface, i.e. once in the channel, and at three different heights inside the GDL. It is readily apparent that the

oxygen fraction oscillates when approaching the membrane. In areas where a fuel channel passes, the current density increases, while the oxygen mass fraction is reduced at the same time.

4.3. **Field of application and limitations of the model.** Even though the model is complex, detailed and three-dimensional, it is important to understand that it has two main limitations: very simplified electrochemical and water transport models. Ignoring water transport in the flow channels and using the unsaturated flow theory will probably underestimate liquid water formation [26]. Moreover, the model requires certain input parameters for the electrochemical model, such as the exchange current density, to be fitted from experiments. Predictions of the cell potential without any measurement data might contain therefore non-negligible error. This limitation is caused on the one hand by the fact that the overpotentials depend on the exact material, assembling and ageing. On the other hand, the electrochemical model is strongly simplified by replacing the three-dimensional reactions in the tiny catalyst layer by simple two-dimensional boundary conditions. The main field of application is therefore not describing electrochemistry on the microscale, but rather providing support in fuel cell design from an engineering perspective. The simplifications outlined above allow for comparably fast simulations to predict important variables such as flow speed and pressure drop. The model allows as well to give an impression of temperature, species and current distribution. It is therefore especially useful in designing the overall setup, the bipolar plates and the flow fields of a fuel cell.

5. Conclusion and future work

5.1. **Summary.** An open-source CFD model for PEM fuel cells has been developed with the motivation to facilitate cooperation, model comparison, extension and validation. This original model is based on the software *openFuelCell* for solid oxide fuel cells; the three-dimensional continum mechanical model accounts for phase change and two-phase transport using unsaturated flow theory, while electrochemistry is based on a Tafel equation and the membrane model on the Springer approach. The steady-state model has been implemented in the open-source CFD library OpenFOAM®v2112. It includes all major physical, chemical and hydrodynamic phenomena, such as flow, mass transfer, electrochemistry, two-phase transport and phase change. In implementing the software, care was taken to structure the code logically into different libraries according to the underlying physics. This not only improves understanding, but also facilitates extensions of the model. User-friendliness, error handling, convergence control, and monitoring at runtime have all been improved compared to the *openFuelCell* model.

The developed model successfully reproduces the polarisation curves of two different PEM fuel cells, which have been operated at CIEMAT and the research centre Jülich. The simulations clearly show the interplay of temperature, liquid water formation and local current density under the ribs of the flow channels. Furthermore, the Nernst potential, humidification and current density along the flow channels illustrate the dependence of the membrane conductivity on water content. In this respect, the simulations provide detailed qualitative and quantitative information about specific practical engineering designs.

The present model can easily be extended and applied to other PEM fuel cells with different geometry. Developed as an engineering toolkit to support practical fuel cell design, the existing runtime selectable sub-models can, and shall be extended by more sophisticated ones by the user. With this aim, the code is released as open-source together with the geometric models of the two PEM fuel cells described above.

5.2. **Outlook.** Fuel cell modelling is an extremely complex process – especially due to the necessary coupling of physical phenomena on different scales. Therefore, model development is a continous process. In this respect, it is planned to improve user friendliness and error handling of the software continously. Concerning the iterative procedure used to obtain the targeted cell voltage or current density, larger relaxation factors and speedup are expected to be possible by using the secant method [122] when updating the current density. Alternatively, linearising strongly non-linear terms such as the Butler-Volmer equation using a Taylor series [123–125] and/or applying a pseudo-transient time-stepping could perhaps be used to improve convergence, also. Moreover, the submodules for the activation, ohmic and concentration overpotentials will be improved further. Concerning mass transport losses, the implementation of a complete Euler-Euler model as alternative to unsaturated flow theory would be desirable – or alternatively an extension of the UFT to water transport in the flow channels [79]. In addition to these modelling tasks, a comprehensive material database for fuel cells would facilitate modelling considerably.

Acknowledgements

This work was supported by the Ministerio de Ciencia e Innovación, Project ELHYPORT (PID2019-110896RB-I00) as well as a postdoctoral fellowship of the German Academic Exchange Service (DAAD).

Fruitful discussions with P. García-Salaberri, B. Naud, D. Fernández, A. Iranzo, C. Jiménez, V. Kourdioumov, P. Personnettaz and T. Weier as well as several excellent suggestions for improving the solver by different referees are gratefully acknowledged.

Author Contributions: Conceptualisation, N.W., S.B.B., W.L., U.R. and A.M.C.; methodology, N.W., L.K., S.B.B., W.L., U.R., S.Z., P.F.-A. and A.M.C.; software, N.W., L.K., U.R. and Z.H.; validation, N.W., L.K., U.R., P.F.-A. and A.M.C.; investigation, N.W., L.K., S.B.B., W.L., U.R., P.F-A. and A.M.C.; writing—original draft preparation, N.W., S.B.B. and A.M.C.; writing—review and editing, N.W., S.B.B. and A.M.C.; visualisation, N.W. and L.K.; supervision, S.B.B. and A.M.C.; funding acquisition, N.W. and A.M.C. All authors have read and agreed to the published version of the manuscript.

Nomenclature

Constants

R	ideal gas constant (8.314 J/K/mol)
F	Faraday constant (96 485 sA/mol)

Scalars

a	activity
a	stoichiometric coefficient reactant
b	Tafel slope (V)
b	stoichiometric coefficient product
c_p	specific heat capacity (J/kg/K)
D	diffusion coefficient (m^2/s)
E	standard potential (V)
E_act	activation energy (J/mol)
G	Gibbs free energy (J)
H	enthalpy (J)
h	latent heat (J/kg)
J	Leverett function
j	current density (A/m^2)
j_0	exchange current density (A/m^2)
K	permeability (m^2)
k	thermal conductivity (W/m/K)
M	molar mass (kg/m^3)
m	mass (kg)
M_m	equivalent weight of the membrane (kg/mol)
N	molar flux ($\mathrm{mol}/\mathrm{m}^2/\mathrm{s}$)
n	reaction order
p	pressure (Pa)
p_c	capillary pressure (Pa)
Q	mass flux ($\mathrm{kg}/\mathrm{m}^2/\mathrm{s}$)
R	area specific resistance ($\Omega\mathrm{m}^2$)
S	entropy (J)
s	liquid water saturation
$S_\mathrm{v-l}$	phase change source term
T	temperature (K)
U	open circuit potential (V)
u	interstitial velocity (m/s)
V	cell potential (V)
x	molar fraction
y	mass fraction
z	coordinate (m)
z	number of electrons

Vectors

$\boldsymbol{g}$	gravity (m^2/s)
$\boldsymbol{u}$	interstitial velocity (m/s)
$\boldsymbol{x}$	coordinate vector (m)

Greek

α	charge transfer coefficient
ΔE	difference of standard potentials
Δ	difference
δ	membrane thickness (m)
η	overpotential (V)
γ	condensation or evaporation rate (1/s)
κ	conductivity (S/m)
λ	membrane water content
λ	stoichiometric ratio of reactants
μ	dynamic viscosity (Pa s)
ν	kinematic viscosity (m^2/s)
ρ	density (kg/m^3)
σ	surface tension (N/m)
θ	contact angle ($^\circ$)
ε	dry porosity
φ	relative humidity (%)
ϑ	temperature ($^\circ\mathrm{C}$)

Subscripts

0	reference value
A	anode
act	activation
C	cathode
cond	condensation
eff	effective
evap	evaporation
m	membrane
sat	saturation
T	thermal
v	vapour
v-l	vapour to liquid
w	water

References

[1] T. E. Springer, T. A. Zawodzinski, and S. Gottesfeld, "Polymer electrolyte fuel cell model," *J. Electrochem. Soc.*, vol. 138, no. 8, pp. 2334–2342, 1991.

[2] D. M. Bernardi and M. W. Verbrugge, "A Mathematical Model of the Solid-Polymer-Electrolyte Fuel Cell," *J. Electrochem. Soc.*, vol. 139, no. 9, pp. 2477–2491, 1992.

[3] S. B. Beale, H.-W. Choi, J. G. Pharoah, H. K. Roth, H. Jasak, and D. H. Jeon, "Open-source computational model of a solid oxide fuel cell," *Comput. Phys. Commun.*, vol. 200, pp. 15–26, 2016.

[4] A. Z. Weber and J. Newman, "Modeling Transport in Polymer-Electrolyte Fuel Cells," *Chem. Rev.*, vol. 104, no. 10, pp. 4679–4726, 2004.

[5] A. Z. Weber, R. L. Borup, R. M. Darling, P. K. Das, T. J. Dursch, W. Gu, D. Harvey, A. Kusoglu, S. Litster, M. M. Mench, R. Mukundan, J. P. Owejan, J. G. Pharoah, M. Secanell, and I. V. Zenyuk, "A Critical Review of Modeling Transport Phenomena in Polymer-Electrolyte Fuel Cells," *J. Electrochem. Soc.*, vol. 161, no. 12, pp. F1254–F1299, 2014.

[6] M. Andersson, S. Beale, M. Espinoza, Z. Wu, and W. Lehnert, "A review of cell-scale multiphase flow modeling, including water management, in polymer electrolyte fuel cells," *Appl. Energy*, vol. 180, pp. 757–778, 2016.

[7] C. Y. Wang and P. Cheng, "A multiphase mixture model for multiphase, multicomponent transport in capillary porous media I. Model development," *Int. J. Heat Mass Transf.*, vol. 39, pp. 3607–3618, 1996.

[8] V. Gurau, R. V. Edwards, J. A. Mann, and T. A. Zawodzinski, "A Look at the Multiphase Mixture Model for PEM Fuel Cell Simulations," *Electrochem. Solid-State Lett.*, vol. 11, no. 8, pp. B132–B135, 2008.

[9] Z. Wang, J. Yang, B. Koo, and F. Stern, "A coupled level set and volume-of-fluid method for sharp interface simulation of plunging breaking waves," *Int. J. Multiph. Flow*, vol. 35, no. 3, pp. 227–246, 2009.

[10] V. Gurau, "Response to "Comment on 'A Look at the Multiphase Mixture Model for PEM Fuel Cell Simulations' " [Electrochem. Solid-State Lett., 11, B132 (2008)]," *Electrochem. Solid-State Lett.*, vol. 12, no. 2, pp. S4–S6, 2009.

[11] S. Mazumder and J. V. Cole, "Rigorous 3-D Mathematical Modeling of PEM Fuel Cells," *J. Electrochem. Soc.*, vol. 150, no. 11, pp. A1510–A1517, 2003.

[12] Y. Wang and C.-Y. Wang, "A Nonisothermal, Two-Phase Model for Polymer Electrolyte Fuel Cells," *J. Electrochem. Soc.*, vol. 153, no. 6, pp. A1193–A1200, 2006.

[13] B. Carnes, D. Spernjak, G. Luo, L. Hao, K. S. Chen, C.-Y. Wang, R. Mukundan, and R. L. Borup, "Validation of a two-phase multidimensional polymer electrolyte membrane fuel cell computational model using current distribution measurements," *J. Power Sources*, vol. 236, pp. 126–137, 2013.

[14] C. Wang and P. Cheng, "Multiphase Flow and Heat Transfer in Porous Media," in *Advances in Heat Transfer*. Academic Press, 1997, vol. 30, pp. 93–196.

[15] W. Wang, X. Zhang, C. Xin, and Z. Rao, "An experimental study on thermal management of lithium ion battery packs using an improved passive method," *Appl. Therm. Eng.*, vol. 134, pp. 163–170, 2018.

[16] M. Abdollahzadeh, P. Ribeirinha, M. Boaventura, and A. Mendes, "Three-dimensional modeling of PEMFC with contaminated anode fuel," *Energy*, vol. 152, pp. 939–959, 2018.

[17] W. He, J. S. Yi, and T. Van Nguyen, "Two-phase flow model of the cathode of PEM fuel cells using interdigitated flow fields," *AIChE J.*, vol. 46, no. 10, pp. 2053–2064, 2000.

[18] F. Jiang, W. Fang, and C.-Y. Wang, "Non-isothermal cold start of polymer electrolyte fuel cells," *Electrochim. Acta*, vol. 53, no. 2, pp. 610–621, 2007.

[19] K. Jiao, "Experimental and Modelling Studies of Cold Start Processes in Proton Exchange Membrane Fuel Cells," Ph.D. dissertation, University of Waterloo, 2011.

[20] K. Jiao and X. Li, "Three-dimensional multiphase modeling of cold start processes in polymer electrolyte membrane fuel cells," *Electrochim. Acta*, vol. 54, no. 27, pp. 6876–6891, 2009.

[21] ——, "Water transport in polymer electrolyte membrane fuel cells," *Prog. Energy Combust. Sci.*, vol. 37, no. 3, pp. 221–291, 2011.

[22] H. Wu, P. Berg, and X. Li, "Modeling of PEMFC Transients with Finite-Rate Phase-Transfer Processes," *J. Electrochem. Soc.*, vol. 157, no. 1, pp. B1–B12, 2010.

[23] H. Wu, X. Li, and P. Berg, "On the modeling of water transport in polymer electrolyte membrane fuel cells," *Electrochim. Acta*, vol. 54, no. 27, pp. 6913–6927, 2009.

[24] T. Berning and N. Djilali, "A 3D, Multiphase, Multicomponent Model of the Cathode and Anode of a PEM Fuel Cell," *J. Electrochem. Soc.*, vol. 150, no. 12, pp. A1589–A1598, 2003.

[25] R. Vetter and J. O. Schumacher, "Free open reference implementation of a two-phase PEM fuel cell model," *Comput. Phys. Commun.*, vol. 234, pp. 223–234, 2019.

[26] U. Pasaogullari and C.-Y. Wang, "Two-phase transport and the role of micro-porous layer in polymer electrolyte fuel cells," *Electrochim. Acta*, vol. 49, no. 25, pp. 4359–4369, 2004.

[27] V. Gurau, H. Liu, and S. Kakaç, "Two-dimensional model for proton exchange membrane fuel cells," *AIChE J.*, vol. 44, no. 11, pp. 2410–2422, 1998.

[28] T. Berning, M. Odgaard, and S. K. Kær, "A Computational Analysis of Multiphase Flow Through PEMFC Cathode Porous Media Using the Multifluid Approach," *J. Electrochem. Soc.*, vol. 156, no. 11, pp. B1301–B1311, 2009.

[29] S. Rahgoshay, A. Ranjbar, A. Ramiar, and E. Alizadeh, "Thermal investigation of a PEM fuel cell with cooling flow field," *Energy*, vol. 134, pp. 61–73, 2017.

[30] S. Beale, Y. Lin, S. Zhubrin, and W. Dong, "Computer methods for performance prediction in fuel cells," *J. Power Sources*, vol. 118, no. 1-2, pp. 79–85, 2003.

[31] W. Ying, T.-H. Yang, W.-Y. Lee, J. Ke, and C.-S. Kim, "Three-dimensional analysis for effect of channel configuration on the performance of a small air-breathing proton exchange membrane fuel cell (PEMFC)," *J. Power Sources*, vol. 145, no. 2, pp. 572–581, 2005.

[32] W. Ying, Y.-J. Sohn, W.-Y. Lee, J. Ke, and C.-S. Kim, "Three-dimensional modeling and experimental investigation for an air-breathing polymer electrolyte membrane fuel cell (PEMFC)," *J. Power Sources*, vol. 145, no. 2, pp. 563–571, 2005.

[33] Y. Wang and M. Ouyang, "Three-dimensional heat and mass transfer analysis in an air-breathing proton exchange membrane fuel cell," *J. Power Sources*, vol. 164, no. 2, pp. 721–729, 2007.

[34] Y. Lin and S. B. Beale, "Numerical Predictions of Transport Phenomena in a Proton Exchange Membrane Fuel Cell," *J. Fuel Cell Sci. Technol.*, vol. 2, no. 4, pp. 213–218, 2005.

[35] D. Schwarz and S. Beale, "Calculations of transport phenomena and reaction distribution in a polymer electrolyte membrane fuel cell," *Int. J. Heat Mass Transf.*, vol. 52, no. 17-18, pp. 4074–4081, 2009.

[36] A. Iranzo, J. M. Gregorio, P. Boillat, and F. Rosa, "Bipolar plate research using Computational Fluid Dynamics and neutron radiography for proton exchange membrane fuel cells," *Int. J. Hydrog. Energy*, vol. 45, no. 22, pp. 12 432–12 442, 2020.

[37] A. Schmitz, C. Ziegler, J. O. Schumacher, M. Tranitz, E. Fontes, and C. Hebling, "Modelling Approach for Planar Self-Breathing PEMFC and Comparison with Experimental Results," *Fuel Cells*, vol. 4, no. 4, pp. 358–364, 2004.

[38] C. Ziegler, A. Schmitz, M. Tranitz, E. Fontes, and J. O. Schumacher, "Modeling Planar and Self-Breathing Fuel Cells for Use in Electronic Devices," *J. Electrochem. Soc.*, vol. 151, no. 12, pp. A2028–A2041, 2004.

[39] M. Secanell, A. Putz, P. Wardlaw, V. Zingan, M. Bhaiya, M. Moore, J. Zhou, C. Balen, and K. Domican, "OpenFCST: An Open-Source Mathematical Modelling Software for Polymer Electrolyte Fuel Cells," *ECS Transactions*, vol. 64, no. 3, pp. 655–680, 2014.

[40] S. Zhang, U. Reimer, Y. Rahim, S. B. Beale, and W. Lehnert, "Numerical Modeling of Polymer Electrolyte Fuel Cells With Analytical and Experimental Validation," *J. Electrochem. Energy Convers. Storage*, vol. 16, no. 3, p. 031002, 2019.

[41] D. Arndt, W. Bangerth, B. Blais, T. C. Clevenger, M. Fehling, A. V. Grayver, T. Heister, L. Heltai, M. Kronbichler, M. Maier, P. Munch, J.-P. Pelteret, R. Rastak, I. Tomas, B. Turcksin, Z. Wang, and D. Wells, "The deal.II library, Version 9.2," *J. Numer. Math.*, vol. 28, no. 3, pp. 131–146, 2020.

[42] C. Robin, M. Gerard, J. d'Arbigny, P. Schott, L. Jabbour, and Y. Bultel, "Development and experimental validation of a PEM fuel cell 2D-model to study heterogeneities effects along large-area cell surface," *Int. J. Hydrog. Energy*, vol. 40, no. 32, pp. 10 211–10 230, 2015.

[43] F. Nandjou, J.-P. Poirot-Crouvezier, M. Chandesris, and Y. Bultel, "A pseudo-3D model to investigate heat and water transport in large area PEM fuel cells – Part 1: Model development and validation," *Int. J. Hydrog. Energy*, vol. 41, no. 34, pp. 15 545–15 561, 2016.

[44] B. Randrianarizafy, P. Schott, M. Chandesris, M. Gerard, and Y. Bultel, "Design optimization of rib/channel patterns in a PEMFC through performance heterogeneities modelling," *Int. J. Hydrog. Energy*, vol. 43, no. 18, pp. 8907–8926, 2018.

[45] H. G. Weller, G. Tabor, H. Jasak, and C. Fureby, "A tensorial approach to computational continuum mechanics using object-oriented techniques," *Comput. Phys.*, vol. 12, no. 6, pp. 620–631, 1998.

[46] V. Novaresio, M. García-Camprubí, S. Izquierdo, P. Asinari, and N. Fueyo, "An open-source library for the numerical modeling of mass-transfer in solid oxide fuel cells," *Comput. Phys. Commun.*, vol. 183, no. 1, pp. 125–146, 2012.
[47] M. García-Camprubí, "Multiphysics Models for the Simulation of Solid Oxide Fuel Cells," Ph.D. dissertation, University of Zaragoza, Zaragoza, 2011.
[48] M. García-Camprubí and N. Fueyo, "Mass transfer in hydrogen-fed anode-supported SOFCs," *Int. J. Hydrog. Energy*, vol. 35, no. 20, pp. 11 551–11 560, 2010.
[49] S. B. Beale, H. K. Roth, A. Le, and D. H. Jeon, "Development of an open source software library for solid oxide fuel cells," National Research Council Canada, Tech. Rep. NRCC 53179, 2013.
[50] "openFuelCell project," http://openfuelcell.sourceforge.net, 2016.
[51] R. T. Nishida, S. B. Beale, and J. G. Pharoah, "Comprehensive computational fluid dynamics model of solid oxide fuel cell stacks," *Int. J. Hydrog. Energy*, vol. 41, pp. 20 592–20 605, 2016.
[52] H. Grimler, "An openFuelCell tutorial," in *Proceedings of CFD with OpenSource Software*. Chalmers University of Technology, 2017.
[53] R. T. Nishida, S. B. Beale, J. G. Pharoah, L. G. J. de Haart, and L. Blum, "Three-dimensional computational fluid dynamics modelling and experimental validation of the Jülich Mark-F solid oxide fuel cell stack," *J. Power Sources*, vol. 373, pp. 203–210, 2018.
[54] Q. Cao, "Modelling of high temperature polymer electrolyte fuel cells," Ph.D. dissertation, RWTH Aachen, 2017.
[55] S. Zhang, U. Reimer, S. Beale, W. Lehnert, and D. Stolten, "Modeling polymer electrolyte fuel cells: A high precision analysis," *Appl. Energy*, vol. 233–234, pp. 1094–1103, 2019.
[56] S. Zhang, S. B. Beale, U. Reimer, R. T. Nishida, M. Andersson, J. G. Pharoah, and W. Lehnert, "Simple and Complex Polymer Electrolyte Fuel Cell Stack Models: A Comparison," *ECS Trans.*, vol. 86, no. 13, pp. 287–300, 2018.
[57] S. Zhang, "Modeling and Simulation of Polymer Electrolyte Fuel Cells," Ph.D. dissertation, RWTH Aachen, 2019.
[58] D. B. P. Harvey, "Development of a Stochastically-driven, Forward Predictive Performance Model for PEMFCs," Ph.D. dissertation, Queen's University, 2017.
[59] L. Knüpfer, "Validierung eines Open-source-Modells für die Simulation von PEM-Brennstoffzellen und Anwendung auf eine luftatmende Brennstoffzelle," Master thesis, TU Dresden, Dresden, 2020.
[60] S. Zhang, S. Beale, U. Reimer, M. Andersson, and W. Lehnert, "Polymer electrolyte fuel cell modeling - A comparison of two models with different levels of complexity," *Int. J. Hydrog. Energy*, vol. 45, no. 38, pp. 19 761–19 777, 2020.
[61] E. J. F. Dickinson and G. Hinds, "The Butler-Volmer Equation for Polymer Electrolyte Membrane Fuel Cell (PEMFC) Electrode Kinetics: A Critical Discussion," *J. Electrochem. Soc.*, vol. 166, no. 4, pp. F221–F231, 2019.
[62] G. F. Pinder and W. G. Gray, *Essentials of Multiphase Flow and Transport in Porous Media: Pinder/Multiphase Flow.* Hoboken, N.J., USA: John Wiley & Sons, Inc., 2008.
[63] C. Y. Wang, W. B. Gu, and B. Liaw, "Micro-Macroscopic Coupled Modeling of Batteries and Fuel Cells," *J. Electrochem. Soc.*, vol. 145, pp. 3407–3417, 1998.
[64] S. Um, C. Y. Wang, and K. S. Chen, "Computational Fluid Dynamics Modeling of Proton Exchange Membrane Fuel Cells," *J. Electrochem. Soc.*, vol. 147, no. 12, pp. 4485–4493, 2000.
[65] Z. H. Wang, C. Y. Wang, and K. S. Chen, "Two-phase flow and transport in the air cathode of proton exchange membrane fuel cells," *J. Power Sources*, vol. 94, pp. 40–50, 2001.
[66] B. Emonts and D. Stolten, *Fuel Cell Science and Engineering.* Wiley-VCH, 2012.
[67] H. Rusche, "Computational Fluid Dynamics of Dispersed Two-Phase Flows at High Phase Fractions," Ph.D. dissertation, Imperial College London, 2002.
[68] N. Weber, P. Beckstein, W. Herreman, G. M. Horstmann, C. Nore, F. Stefani, and T. Weier, "Sloshing instability and electrolyte layer rupture in liquid metal batteries," *Phys. Fluids*, vol. 29, no. 5, p. 054101, 2017.
[69] S. Whitaker, "The Forchheimer equation: A theoretical development," *Transp. Porous Media*, vol. 25, no. 1, pp. 27–61, 1996.
[70] J. T. Gostick, M. W. Fowler, M. A. Ioannidis, M. D. Pritzker, Y. Volfkovich, and A. Sakars, "Capillary pressure and hydrophilic porosity in gas diffusion layers for polymer electrolyte fuel cells," *J. Power Sources*, vol. 156, no. 2, pp. 375–387, 2006.
[71] Q. Ye and T. V. Nguyen, "Three-Dimensional Simulation of Liquid Water Distribution in a PEMFC with Experimentally Measured Capillary Functions," *J. Electrochem. Soc.*, vol. 154, no. 12, pp. B1242–B1251, 2007.

[72] S. B. Beale, D. H. Schwarz, M. R. Malin, and D. B. Spalding, "Two-phase flow and mass transfer within the diffusion layer of a polymer electrolyte membrane fuel cell," *Comput. Therm. Sci.*, vol. 1, no. 2, pp. 105–120, 2009.

[73] E. N. Fuller, P. D. Schettler, and J. C. Giddings, "New method for prediction of binary gas-phase diffusion coefficients," *Ind. Eng. Chem.*, vol. 58, no. 5, pp. 18–27, 1966.

[74] D. Spalding, "A standard formulation of the steady convective mass transfer problem," *Int. J. Heat Mass Transf.*, vol. 1, no. 2-3, pp. 192–207, 1960.

[75] S. Beale, "Calculation procedure for mass transfer in fuel cells," *J. Power Sources*, vol. 128, no. 2, pp. 185–192, 2004.

[76] S. B. Beale, "Mass transfer formulation for polymer electrolyte membrane fuel cell cathode," *Int. J. Hydrog. Energy*, vol. 40, no. 35, pp. 11 641–11 650, 2015.

[77] S. B. Beale, U. Reimer, D. Froning, H. Jasak, M. Andersson, J. G. Pharoah, and W. Lehnert, "Stability Issues of Fuel Cell Models in the Activation and Concentration Regimes," *J. Electrochem. Energy Convers. Storage*, vol. 15, no. 4, p. 041008, 2018.

[78] S. B. Beale, S. Zhang, M. Andersson, R. T. Nishida, J. G. Pharoah, and W. Lehnert, "Heat and Mass Transfer in Fuel Cells and Stacks," in *50 Years of CFD in Engineering Sciences: A Commemorative Volume in Memory of D. Brian Spalding*, A. K. Runchal, Ed. Springer Singapore, 2020, pp. 485–511.

[79] Y. Wang, S. Basu, and C.-Y. Wang, "Modeling two-phase flow in PEM fuel cell channels," *J. Power Sources*, vol. 179, no. 2, pp. 603–617, 2008.

[80] D. Natarajan and T. Van Nguyen, "A Two-Dimensional, Two-Phase, Multicomponent, Transient Model for the Cathode of a Proton Exchange Membrane Fuel Cell Using Conventional Gas Distributors," *J. Electrochem. Soc.*, vol. 148, no. 12, pp. A1324–A1335, 2001.

[81] D. R. Lide, Ed., *CRC Handbook of Chemistry and Physics*. CRC Press, 2005.

[82] C.-Y. Wang and C. Beckermann, "A two-phase mixture model of liquid-gas flow and heat transfer in capillary porous media-l. Formulation," *Int. J. Heat Mass Transf.*, vol. 36, pp. 2747–2758, 1993.

[83] M. Leverett, "Capillary Behavior in Porous Solids," *Trans. AIME*, vol. 142, no. 01, pp. 152–169, 1941.

[84] S. Motupally, A. J. Becker, and J. W. Weidner, "Diffusion of Water in Nafion 115 Membranes," *J. Electrochem. Soc.*, vol. 147, no. 9, pp. 3171–3177, 2000.

[85] J. Milewski, Ed., *Advanced Methods of Solid Oxide Fuel Cell Modeling*, ser. Green Energy and Technology. London: Springer, 2011.

[86] Y. Wang, K. S. Chen, J. Mishler, S. C. Cho, and X. C. Adroher, "A review of polymer electrolyte membrane fuel cells: Technology, applications, and needs on fundamental research," *Appl. Energy*, vol. 88, no. 4, pp. 981–1007, 2011.

[87] C. Turan, "Investigations on the Effect of Manufacturing on the Contact Resistance Behavior of Metallic Bipolar Plates for Polymer Electrolyte Membrane Fuel Cells," Ph.D. dissertation, Virginia Commonwealth University, 2011.

[88] S. Lædre, O. E. Kongstein, A. Oedegaard, F. Seland, and H. Karoliussen, "Measuring In Situ Interfacial Contact Resistance in a Proton Exchange Membrane Fuel Cell," *J. Electrochem. Soc.*, vol. 166, no. 13, pp. F853–F859, 2019.

[89] Y. Zhou, G. Lin, A. Shih, and S. Hu, "A micro-scale model for predicting contact resistance between bipolar plate and gas diffusion layer in PEM fuel cells," *J. Power Sources*, vol. 163, no. 2, pp. 777–783, 2007.

[90] S. El Oualid, R. Lachat, D. Candusso, and Y. Meyer, "Characterization process to measure the electrical contact resistance of Gas Diffusion Layers under mechanical static compressive loads," *Int. J. Hydrog. Energy*, vol. 42, no. 37, pp. 23 920–23 931, 2017.

[91] V. Mishra, F. Yang, and R. Pitchumani, "Measurement and Prediction of Electrical Contact Resistance Between Gas Diffusion Layers and Bipolar Plate for Applications to PEM Fuel Cells," *J. Fuel Cell Sci. Technol.*, vol. 1, no. 1, pp. 2–9, 2004.

[92] C. J. Netwall, B. D. Gould, J. A. Rodgers, N. J. Nasello, and K. E. Swider-Lyons, "Decreasing contact resistance in proton-exchange membrane fuel cells with metal bipolar plates," *J. Power Sources*, vol. 227, pp. 137–144, 2013.

[93] A. J. Bard and L. R. Faulkner, *Electrochemical Methods: Fundamentals and Applications*, 2nd ed. New York: Wiley, 2001.

[94] J. Newman and K. E. Thomas-Alyea, *Electrochemical Systems*. John Wiley & Sons, 2004.

[95] K. J. Vetter, *Electrochemical Kinetics*. Burlington: Elsevier Science, 1967.

[96] K. C. Neyerlin, W. Gu, J. Jorne, and H. A. Gasteiger, "Determination of Catalyst Unique Parameters for the Oxygen Reduction Reaction in a PEMFC," *J. Electrochem. Soc.*, vol. 153, no. 10, pp. A1955–A1963, 2006.

[97] A. Leonide, "SOFC Modelling and Parameter Identification by means of Impedance Spectroscopy," Ph.D. dissertation, Universität Karlsruhe, 2010.

[98] M. García-Camprubí, S. Izquierdo, and N. Fueyo, "Challenges in the electrochemical modelling of solid oxide fuel and electrolyser cells," *Renew. Sustain. Energy Rev.*, vol. 33, pp. 701–718, 2014.

[99] W. H. Press, S. A. Teukolsky, W. T. Vetterling, and B. P. Flannery, *Numerical Recipes in C*. Cambridge University Press, 1992.

[100] D. A. G. Bruggeman, "Berechnung verschiedener physikalischer Konstanten von heterogenen Substanzen. I. Dielektrizitätskonstanten und Leitfähigkeiten der Mischkörper aus isotropen Substanzen," *Ann. Phys.*, vol. 416, no. 7, pp. 636–664, 1935.

[101] N. Weber, P. Beckstein, V. Galindo, M. Starace, and T. Weier, "Electro-vortex flow simulation using coupled meshes," *Comput. Fluids*, vol. 168, pp. 101–109, 2018.

[102] N. Weber, S. Landgraf, K. Mushtaq, M. Nimtz, P. Personnettaz, T. Weier, J. Zhao, and D. Sadoway, "Modeling discontinuous potential distributions using the finite volume method, and application to liquid metal batteries," *Electrochim. Acta*, vol. 318, pp. 857–864, 2019.

[103] J. Kim, G. Luo, and C.-Y. Wang, "Modeling liquid water re-distributions in bi-porous layer flow-fields of proton exchange membrane fuel cells," *J. Power Sources*, vol. 400, pp. 284–295, 2018.

[104] P. Havaej, "A numerical investigation of the performance of Polymer Electrolyte Membrane fuel cell with the converging-diverging flow field using two-phase flow modeling," *Energy*, vol. 182, pp. 656–672, 2019.

[105] Y. Shi, H. Janßen, and W. Lehnert, "A Transient Behavior Study of Polymer Electrolyte Fuel Cells with Cyclic Current Profiles," *Energies*, vol. 12, p. 2370, 2019.

[106] X. Ye and C.-Y. Wang, "Measurement of Water Transport Properties Through Membrane-Electrode Assemblies," *J. Electrochem. Soc.*, vol. 154, no. 7, pp. B676–B686, 2007.

[107] R. Schweiss, "Benefits of Membrane Electrode Assemblies with Asymmetrical GDL Configurations for PEM Fuel Cells," *Fuel Cells*, vol. 16, no. 1, pp. 100–106, 2016.

[108] O. Burheim, P. J. Vie, S. Møller-Holst, J. Pharoah, and S. Kjelstrup, "A calorimetric analysis of a polymer electrolyte fuel cell and the production of H_2O_2 at the cathode," *Electrochim. Acta*, vol. 55, no. 3, pp. 935–942, 2010.

[109] O. Burheim, P. Vie, J. Pharoah, and S. Kjelstrup, "Ex situ measurements of through-plane thermal conductivities in a polymer electrolyte fuel cell," *J. Power Sources*, vol. 195, no. 1, pp. 249–256, 2010.

[110] Freudenberg, "Freudenberg Gas Diffusion Layers (Datasheet)," Freudenberg Performance Materials SE & Co. KG, Tech. Rep., 2020.

[111] M. V. Williams, E. Begg, L. Bonville, H. R. Kunz, and J. M. Fenton, "Characterization of Gas Diffusion Layers for PEMFC," *J. Electrochem. Soc.*, vol. 151, no. 8, pp. A1173–A1180, 2004.

[112] A. M. Chaparro, M. A. Folgado, P. Ferreira-Aparicio, A. J. Martín, I. Alonso-Álvarez, and L. Daza, "Properties of Catalyst Layers for PEMFC Electrodes Prepared by Electrospray Deposition," *J. Electrochem. Soc.*, vol. 157, no. 7, pp. B993–B999, 2010.

[113] A. El-Kharouf, T. J. Mason, D. J. Brett, and B. G. Pollet, "Ex-situ characterisation of gas diffusion layers for proton exchange membrane fuel cells," *J. Power Sources*, vol. 218, pp. 393–404, 2012.

[114] International Atomic Energy Agency, *Thermophysical Properties of Materials for Nuclear Engineering: A Tutorial and Collection of Data*. Vienna: International Atomic Energy Agency, 2008.

[115] Y. Shi, "Stationary and Transient Behaviour of Polymer Electrolyte Fuel Cells," Ph.D. dissertation, RWTH Aachen, 2021.

[116] U. Reimer, W. Lehnert, Y. Holade, and B. Kokoh, "Irreversible Losses in Fuel Cells," in *Fuel Cells and Hydrogen*. Elsevier, 2018, pp. 15–40.

[117] P. Ferreira-Aparicio and A. M. Chaparro, "Influence of the cathode catalyst layer thickness on the behaviour of an air breathing PEM fuel cell," *Adv. Energy Res.*, vol. 2, no. 2, pp. 73–84, 2014.

[118] J. J. Conde, M. A. Folgado, P. Ferreira-Aparicio, A. M. Chaparro, A. Chowdhury, A. Kusoglu, D. Cullen, and A. Z. Weber, "Mass-transport properties of electrosprayed Pt/C catalyst layers for polymer-electrolyte fuel cells," *J. Power Sources*, vol. 427, pp. 250–259, 2019.

[119] M. A. Folgado, J. J. Conde, P. Ferreira-Aparicio, and A. M. Chaparro, "Single Cell Study of Water Transport in PEMFCs with Electrosprayed Catalyst Layers," *Fuel Cells*, vol. 18, no. 5, pp. 602–612, 2018.

[120] Y. Ho and T. K. Chu, "Electrical Resistivity and Thermal Conductivity of Nine Selected AISI stainless Steels," American Iron and Steel Institute, CINDAS Report 45, 1977.
[121] M. A. Folgado, P. Ferreira-Aparicio, and A. M. Chaparro, "An optical and single cell study of the assembly of a PEMFC with dry and expanded Nafion," *Int. J. Hydrog. Energy*, vol. 41, no. 1, pp. 505–515, 2016.
[122] M. Avriel, *Nonlinear Programming: Analysis and Methods*. Englewood Cliffs: Prentice-Hall, 1976.
[123] A. N. Colli and H. H. Girault, "Compact and General Strategy for Solving Current and Potential Distribution in Electrochemical Cells Composed of Massive Monopolar and Bipolar Electrodes," *J. Electrochem. Soc.*, vol. 164, no. 11, pp. E3465–E3472, 2017.
[124] A. Colli and J. Bisang, "Current and potential distribution in electrochemical reactors with activated or resistive electrodes. A multiregion and open source approach," *Electrochim. Acta*, vol. 290, pp. 676–685, 2018.
[125] A. N. Colli and J. M. Bisang, "Editors' Choice—Coupling k Convection-Diffusion and Laplace Equations in an Open-Source CFD Model for Tertiary Current Distribution Calculations," *J. Electrochem. Soc.*, vol. 167, no. 1, p. 013513, 2020.